Journal of Fluids and Structures 22 (2006) 1079–1096

JOURNAL OF
FLUIDS AND
STRUCTURES

www.elsevier.com/locate/jfs

Hydroelastic vibration of two annular plates coupled with a bounded compressible fluid

Kyeong-Hoon Jeong*

Mechanical Engineering Division, Korea Atomic Energy Research Institute, P.O. Box 105, Yuseong, Daejeon 305-600, Republic of Korea

Received 12 July 2005; accepted 13 July 2006

Abstract

A theoretical study on a linear hydroelastic vibration of two annular plates coupled with a bounded fluid is presented. The proposed method, based on the Rayleigh–Ritz method and the finite Hankel transform, is verified through a finite element analysis by using a commercial computer code, with an excellent accuracy. It is assumed that plates with an unequal thickness and with an unequal inner radius are clamped along their edges and an inviscid compressible fluid fills the space between the annular plates and the outer rigid vessel. When the two annular plates are identical, distinct in-phase and out-of-phase modes are observed. By increasing the difference in the plate thickness, the symmetric in-phase and out-of-phase modes with respect to the middle plane of the system are gradually shifted to pseudo in-phase and out-of-phase modes, and eventually they are changed to mixed modes. It is found that the natural frequencies decrease with an increase of the fluid compressibility, and additional modes due to a fluid concentration are observed when the plates are coupled with a compressible fluid. The fluid compressibility effect on the natural frequency is dominant in the out-of-phase modes and the higher modes. Also, the effects of the fluid thickness or the distance between the plates and the inner radius of the plates on the natural frequencies of the wet modes are investigated.

1. Introduction

Annular plates are one of the most common kind of components used in mechanical and structural engineering. In recent literature, there has been renewed interest in the problem of plates vibrating in contact with water. For example, multiple circular or annular plates in contact with a coolant have been used in an integral-type nuclear reactor for irradiation shielding. It was found that the dynamic characteristics of the multiple circular plates were changed because of the presence of coolant fluid gaps between the plates (Jeong et al., 2001).

Kasahara et al. (1994) calculated the natural frequencies of two circular plates coupled with a fluid and they verified them by experiment. They suggested an analytical method based on a matrix size reduction by introducing a modal method for both the structure and the fluid. Amabili et al. (1996) studied the hydroelastic vibration of an annular plate in contact with an infinite fluid by using the Rayleigh–Ritz method based on the mode expansion of dry mode shapes. For the case of a fluid domain with finite depth, Amabili (1996) investigated the free vibration of an annular plate in contact with water on one side by using the Rayleigh–Ritz method, based on the assumed mode approach. Amabili and

---

*Tel.: +82 42 868 8792.
E-mail address: khjeong@kaeri.re.kr.

doi:10.1016/j.jfluidstructs.2006.07.001

Dalpiaz (1998) developed a theory for vibrations of an annular plate glued to a liquid-filled annular cylindrical tank and carried out an experiment to verify their theory. Amabili (2000a) also theoretically investigated the free vibration of a fluid-filled hermetic can composed of a circular cylindrical flexible shell and two circular end-plates by using the Rayleigh–Ritz method. Cho et al. (2002) studied the modal characteristics of a liquid storage tank baffled with an annular plate by the coupled structural–acoustic finite element method (FEM). Theoretical and experimental studies on the natural frequencies of free-edge annular plates resting on a free surface or completely submerged were carried out by Kwak and Amabili (1999). They considered an unbounded fluid domain and they also introduced nondimensionalized added virtual mass incremental (NAVMI) factors in order to estimate the fluid effect on the individual natural frequencies of the fluid–structure system. Liang et al. (1999) theoretically examined annular plates placed on the fluid domain which is an annular aperture in an infinite rigid wall by applying the Hankel transformation. However, all the work outlined above, deals with a single annular plate. Jeong (2003) theoretically examined the free vibration of two identical circular plates coupled with a bounded incompressible fluid by using the Rayleigh–Ritz method. Recently, Biswal et al. (2004) studied the dynamic response of a liquid-filled cylindrical tank with an annular baffle by using a finite element formulation, and Kim and Lee (2005) developed an analytical solution for the same problem.

In spite of these many researches on the hydroelastic vibration problem, there has been no attempt to tackle the problem described in the present paper, and the researchers mentioned above have also ignored the effect of fluid compressibility on the modal characteristics of annular plates. Especially, in a light water cooled nuclear reactor, it is known that the coolant density is reduced to about 70% and the coolant bulk modulus is also reduced by about 20% under normal operational conditions. Such a change in the compressibility and the density of the coolant can cause a remarkable difference in the dynamic characteristics of a structure submerged therein. This paper is concerned with the coupling effect of a fluid on the free vibration characteristics of two annular plates with an unequal geometry and clamped boundary conditions. A compressible and frictionless fluid is assumed to be bounded by the outer rigid vessel in the radial direction. The inner radius effect of the annular plates on the natural frequencies is also studied. The natural frequency of each mode under wet conditions is normalized with respect to the natural frequency of the dry mode to estimate the relative hydrodynamic effect for the case of identical annular plates. Also investigated is the effect of a fluid gap between the plates on the natural frequency of the wet condition.

2. Theoretical background

2.1. Formulation for two annular plates

Fig. 1 shows two annular plates coupled with a compressible fluid, where R, h_1, and h_2 ($\ll R$) represent the outer radius, the thickness of the upper and the lower annular plates, respectively. The inner radius of the upper annular plate is denoted by a, and the lower one is referred to as b. The fluid is radially bounded by an outer rigid cylindrical vessel

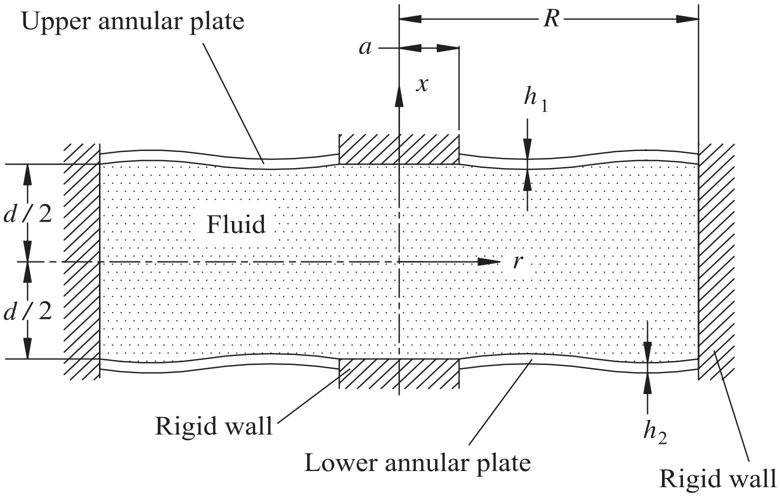

Fig. 1. Two annular plates coupled with a compressible fluid.

and each annular plate is clamped along its inner and outer edges. For a simple formulation of the theory, the gravity effect is neglected. The upper annular plate is referred to by the subscript "1", while the lower one by the subscript "2."

In the Rayleigh–Ritz method, each individual wet mode shape can be expanded in a series by using a finite number of admissible functions, W_{nmj} ($m = 1, 2, \ldots, M$) and appropriate unknown coefficients q_m and p_m. Since the dry mode shapes of an annular plate are selected as admissible functions in the theory, individual wet transverse displacements of the annular plates for an arbitrary nodal diameter n ($n = 0, 1, 2, \ldots$), can be written in the form of

$$w_1(r,\theta,t) = w_1(r,\theta)\exp(\mathrm{i}\omega t) = \cos(n\theta)\sum_{m=1}^{M} q_m W_{nm}(r)\exp(\mathrm{i}\omega t) \quad \text{for the upper plate,} \tag{1a}$$

$$w_2(r,\theta,t) = w_2(r,\theta)\exp(\mathrm{i}\omega t) = \cos(n\theta)\sum_{m=1}^{M} p_m W_{nm}(r)\exp(\mathrm{i}\omega t) \quad \text{for the lower plate,} \tag{1b}$$

where $\mathrm{i} = \sqrt{-1}$, ω is the natural frequency of the fluid-coupled annular plates, and t is the time. The dry eigenfunctions of an annular plate in air are thus expressed as follows:

$$W_{nm}(r) = \mathrm{J}_n(\lambda_{nm}r) + A_{nm}\mathrm{Y}_n(\lambda_{nm}r) + B_{nm}\mathrm{I}_n(\lambda_{nm}r) + C_{nm}\mathrm{K}_n(\lambda_{nm}r), \tag{2}$$

where A_{nm}, B_{nm} and C_{nm} are the arbitrary modal constants which can be determined by the plate boundary conditions. J_n and I_n are the Bessel functions and the modified Bessel functions of the first kind, and Y_n and K_n are the Bessel functions and the modified Bessel functions of the second kind, respectively. Before determining the natural frequencies of the fluid–structure coupled system, we should consider the clamped geometric boundary condition of the upper annular plate displacement. The transverse displacement, W_{nm}, should disappear at $r = R$ and $r = a$. Therefore,

$$\mathrm{J}_n(\lambda_{nm}a) + A_{nm}\mathrm{Y}_n(\lambda_{nm}a) + B_{nm}\mathrm{I}_n(\lambda_{nm}a) + C_{nm}\mathrm{K}_n(\lambda_{nm}a) = 0, \tag{3}$$

$$\mathrm{J}_n(\lambda_{nm}R) + A_{nm}\mathrm{Y}_n\,(\lambda_{nm}R) + B_{nm}\mathrm{I}_n(\lambda_{nm}R) + C_{nm}\mathrm{K}_n(\lambda_{nm}R) = 0. \tag{4}$$

When we consider another geometric boundary condition with a zero slope along the inner and outer edges of the upper annular plate, the following equations can be obtained:

$$\mathrm{J}'_n(\lambda_{nm}a) + A_{nm}\mathrm{Y}'_n(\lambda_{nm}a) + B_{nm}\mathrm{I}'_n(\lambda_{nm}a) + C_{nm}\mathrm{K}'_n(\lambda_{nm}a) = 0, \tag{5}$$

$$\mathrm{J}'_n(\lambda_{nm}R) + A_{nm}\mathrm{Y}'_n(\lambda_{nm}R) + B_{nm}\mathrm{I}'_n(\lambda_{nm}R) + C_{nm}\mathrm{K}'_n(\lambda_{nm}R) = 0. \tag{6}$$

From the boundary conditions described by Eqs. (3)–(6), the characteristic equation for the dry modes can be simplified by the following determinant form:

$$\begin{vmatrix} \mathrm{J}_n(\lambda_{nm}a) & \mathrm{Y}_n(\lambda_{nm}a) & \mathrm{I}_n(\lambda_{nm}a) & \mathrm{K}_n(\lambda_{nm}a) \\ \mathrm{J}_n(\lambda_{nm}R) & \mathrm{Y}_n(\lambda_{nm}R) & \mathrm{I}_n(\lambda_{nm}R) & \mathrm{K}_n(\lambda_{nm}R) \\ \mathrm{J}'_n(\lambda_{nm}a) & \mathrm{Y}'_n(\lambda_{nm}a) & \mathrm{I}'_n(\lambda_{nm}a) & \mathrm{K}'_n(\lambda_{nm}a) \\ \mathrm{J}'_n(\lambda_{nm}R) & \mathrm{Y}'_n(\lambda_{nm}R) & \mathrm{I}'_n(\lambda_{nm}R) & \mathrm{K}'_n(\lambda_{nm}R) \end{vmatrix} = 0. \tag{7}$$

The modal constants, A_{nm}, B_{nm} and C_{nm} can be derived from the boundary conditions of Eqs. (3)–(6) as listed in Appendix A. The frequency parameter for the lower annular plate can also be calculated by replacing b instead of a in Eq. (7).

2.2. Displacement potential for a fluid

The inner space surrounded by two annular plates, the rigid walls and the vessel is filled with an inviscid and compressible fluid as illustrated in Fig. 1. Each opposite facing side of the annular plates is in contact with the fluid. The fluid oscillation induced by a vibration of the plates can be described with a velocity potential that satisfies the Helmholz equation:

$$\nabla^2\Phi(r,\theta,x,t) = \Phi(r,\theta,x,t)_{,tt}/c^2, \tag{8}$$

where c is the sound speed in the fluid medium and ∇^2 is the Laplacian operator in the polar coordinates r and θ. The velocity potential function Φ can be separated into the displacement potential $\phi(r,\theta,x)$ and the harmonic time function. Thus,

$$\Phi(x,r,\theta,t) = \mathrm{i}\omega\phi(r,\theta,x)\,\exp(\mathrm{i}\omega t). \tag{9}$$

Eq. (8) can be solved in cylindrical coordinates by using the separation of variables method with respect to r, θ, and x for an arbitrary nodal diameter n. Because the displacement potential at $r = 0$ must be finite, the term involving Y_n must be discarded in order to avoid a singularity of the fluid displacement at $r = 0$. This leads to the following solution:

$$\phi(r,\theta,x) = \cos(n\theta)\sum_{s=1}^{\infty}\mathrm{J}_n(\beta_{ns}r)[E_{ns}\sinh(\alpha_{ns}x) + F_{ns}\cosh(\alpha_{ns}x)], \tag{10}$$

where E_{ns} and F_{ns} are the unknown constants describing the fluid motion, and a coefficient β_{ns} can be determined by the fluid boundary condition of Eq. (12). Here, the coefficient β_{ns} is related to coefficient α_{ns} by

$$\beta_{ns}^2 = \alpha_{ns}^2 + (\omega/c)^2. \tag{11}$$

The radial displacement of the fluid must disappear at $r = R$, because the rigid cylindrical vessel has an impermeable wall; i.e.,

$$\left.\frac{\partial\phi(r,\theta,x)}{\partial r}\right|_{r=R} = 0. \tag{12}$$

Therefore, the coefficient, β_{ns} can be determined for a fixed n by inserting Eq. (10) into Eq. (12), thus through

$$\mathrm{J}_n'(\beta_{ns}R) = 0. \tag{13}$$

In order to determine the unknown coefficients E_{ns} and F_{ns} in Eq. (10), compatibility conditions at the interfaces of the upper and the lower annular plates with the fluid should be used. As the transverse displacement of each plate should be identical to a normal displacement of the fluid, the dual compatibility conditions can be written as

$$\left.\frac{\partial\phi(r,\theta,x)}{\partial x}\right|_{x=d/2} = \begin{bmatrix} 0 & r\leqslant a, \\ w_1(r,\theta) & a<r\leqslant R, \end{bmatrix} \tag{14a}$$

$$\left.\frac{\partial\phi(r,\theta,x)}{\partial x}\right|_{x=-d/2} = \begin{bmatrix} 0 & r\leqslant b, \\ w_2(r,\theta) & b<r\leqslant R. \end{bmatrix} \tag{14b}$$

Substituting Eqs. (1a, b), (2) and (10) into Eqs. (14a,b) and integrating term by term after multiplying by $r\mathrm{J}_n(\beta_{ns}r)$ in the interval $(0, R)$ for the finite Hankel transform, we produce

$$\begin{aligned}&\int_a^R\sum_{m=1}^{M}q_m\sum_{s=1}^{\infty}[\mathrm{J}_n(\lambda_{nm}r) + A_{nm}\mathrm{Y}_n(\lambda_{nm}r) + B_{nm}\mathrm{I}_n(\lambda_{nm}r) + C_{nm}\mathrm{K}_n(\lambda_{nm}r)]r\mathrm{J}_n(\beta_{ns}r)\,\mathrm{d}r \\ &\quad = \int_0^R\sum_{s=1}^{\infty}\alpha_{ns}\mathrm{J}_n(\beta_{ns}r)[E_{ns}\cosh(\alpha_{ns}x) + F_{ns}\sinh(\alpha_{ns}x)]r\mathrm{J}_n(\beta_{ns}r)\,\mathrm{d}r,\end{aligned} \tag{15a}$$

$$\begin{aligned}&\int_b^R\sum_{m=1}^{M}p_m\sum_{s=1}^{\infty}[\mathrm{J}_n(\lambda_{nm}r) + A_{nm}\mathrm{Y}_n(\lambda_{nm}r) + B_{nm}\mathrm{I}_n(\lambda_{nm}r) + C_{nm}K_n(\lambda_{nm}r)]r\mathrm{J}_n(\beta_{ns}r)\,\mathrm{d}r \\ &\quad = \int_0^R\sum_{s=1}^{\infty}\alpha_{ns}\mathrm{J}_n(\beta_{ns}r)[E_{ns}\cosh(\alpha_{ns}x) + F_{ns}\sinh(\alpha_{ns}x)]r\mathrm{J}_n(\beta_{ns}r)\,\mathrm{d}r.\end{aligned} \tag{15b}$$

From the orthogonality property of the weighting function, $r\mathrm{J}_n(\beta_{ns}r)$, one can write

$$\begin{aligned}&\sum_{m=1}^{M}q_m\sum_{s=1}^{\infty}[\Lambda1_{nms} + A_{nm}\Lambda2_{nms} + B_{nm}\Lambda3_{nms} + C_{nm}\Lambda4_{nms}] \\ &\quad = \sum_{s=1}^{\infty}\alpha_{ns}H_{ns}\left[E_{ns}\cosh(\alpha_{ns}d/2) + F_{ns}\sinh(\alpha_{ns}d/2)\right],\end{aligned} \tag{16a}$$

$$\begin{aligned}&\sum_{m=1}^{M}p_m\sum_{s=1}^{\infty}[\Lambda1_{nms} + A_{nm}\Lambda2_{nms} + B_{nm}\Lambda3_{nms} + C_{nm}\Lambda4_{nms}] \\ &\quad = \sum_{s=1}^{\infty}\alpha_{ns}H_{ns}\left[E_{ns}\cosh(\alpha_{ns}d/2) - F_{ns}\sinh(\alpha_{ns}d/2)\right],\end{aligned} \tag{16b}$$

where the derived values of $\Lambda 1_{nms}$, $\Lambda 2_{nms}$, $\Lambda 3_{nms}$, $\Lambda 4_{nms}$ and H_{ns} are also listed in Appendix A. Therefore, the displacement potential of the fluid can now be expressed in terms of the unknown coefficients q_m and p_m, instead of the unknown coefficients E_{ns} and F_{ns} in accordance with

$$E_{ns} = \frac{\sum_{m=1}^{M}(q_m + p_m)\eta_{nms}}{2\alpha_{ns}\cosh(\alpha_{ns}d/2)}, \quad F_{ns} = \frac{\sum_{m=1}^{M}(q_m - p_m)\eta_{nms}}{2\alpha_{ns}\cosh(\alpha_{ns}d/2)}, \tag{17a,b}$$

$$\eta_{nms} = \frac{(\Lambda 1_{nms} + A_{nm}\Lambda 2_{nms} + B_{nm}\Lambda 3_{nms} + C_{nm}\Lambda 4_{nms})}{H_{ns}}. \tag{17c}$$

Eventually, the displacement potential of the compressible fluid can be reduced by substituting Eqs. (17a,b) into Eq. (10), yielding

$$\phi(r,\theta,x) = \cos(n\theta)\sum_{m=1}^{M}\sum_{s=1}^{\infty}\eta_{nms}\{q_m N_{ns}(x) + p_m M_{ns}(x)\}\mathrm{J}_n(\beta_{ns}r), \tag{18}$$

where

$$N_{ns}(x) = \frac{1}{2\alpha_{ns}}\left\{\frac{\sinh(\alpha_{ns}x)}{\cosh(\alpha_{ns}d/2)} + \frac{\cosh(\alpha_{ns}x)}{\sinh(\alpha_{ns}d/2)}\right\}, \tag{19a}$$

$$M_{ns}(x) = \frac{1}{2\alpha_{ns}}\left\{\frac{\sinh(\alpha_{ns}x)}{\cosh(\alpha_{ns}d/2)} - \frac{\cosh(\alpha_{ns}x)}{\sinh(\alpha_{ns}d/2)}\right\}. \tag{19b}$$

2.3. Method of a solution

It is useful to introduce the Rayleigh quotient, as already suggested by Zhu (1994) and Amabili (2000b) for a generalized fluid–structure interaction problem, and also applied to a circular plate submerged in a compressible fluid by Jeong and Kim (2005). When the gravity effect is neglected, we can obtain a simplified form

$$\omega^2 = \frac{V_p}{T_p^* + U_F^*}, \tag{20}$$

where V_p is the strain energy of the plates, and the reference kinetic energy of the plates is denoted by T_p^*. The fluid energy term U_F^* includes the kinetic and the potential energies of the compressible fluid and it can be evaluated from a fluid surface motion:

$$\begin{aligned} U_F^* &= \tfrac{1}{2}\rho_o\int_0^{2\pi}\int_a^R\left(\frac{\partial\phi(r,d/2)}{\partial x}\right)\phi(r,d/2)\cos^2(n\theta)r\,\mathrm{d}r\,\mathrm{d}\theta \\ &+ \tfrac{1}{2}\rho_o\int_0^{2\pi}\int_b^R\left(\frac{\partial\phi(r,-d/2)}{\partial x}\right)\phi(r,-d/2)\cos^2(n\theta)r\,\mathrm{d}r\,\mathrm{d}\theta, \end{aligned} \tag{21}$$

where ρ_o is the fluid mass density. Eq. (21) is simplified by an application of Eqs. (14a) and (14b) to

$$U_F^* = \tfrac{1}{2}\rho_o\kappa_\theta\left(\int_a^R w_1\xi(r,d/2)r\,\mathrm{d}r + \int_b^R w_2\xi(r,-d/2)r\,\mathrm{d}r\right), \tag{22}$$

where

$$\phi(r,\theta,x) = \cos(n\theta)\xi(r,x), \tag{23a}$$

$$\kappa_\theta = \begin{bmatrix} 2\pi & \text{for } n = 0, \\ \pi & \text{for } n > 0. \end{bmatrix} \tag{23b}$$

For the numerical calculations for each fixed n value, a sufficiently large finite number of the terms must be considered in all the previous expansions. To solve Eq. (20) numerically, it is also necessary to provide a matrix representation. Hence, the column vectors $\boldsymbol{q}$, $\boldsymbol{p}$ and $\boldsymbol{Q}$ of the unknown coefficients are introduced as follows:

$$\boldsymbol{q} = \{q_1 \quad q_2 \quad q_3 \quad \cdots \quad q_M\}^{\mathrm{T}}, \tag{24a}$$

$$\boldsymbol{p} = \{p_1 \quad p_2 \quad p_3 \quad \cdots \quad p_M\}^{\mathrm{T}}, \tag{24b}$$

$$\boldsymbol{Q} = \begin{Bmatrix} \boldsymbol{q} \\ \boldsymbol{p} \end{Bmatrix}. \tag{24c}$$

Substituting Eqs. (1a), (1b), (2), (18) and (24a)–(24c) into Eq. (22) gives

$$U_F^* = \rho_o \kappa_\theta \boldsymbol{Q}^{\mathrm{T}} \boldsymbol{G} \boldsymbol{Q}, \tag{25}$$

where the $2M \times 2M$ fluid energy matrix, $\boldsymbol{G}$ is obtained by performing an integration of Eq. (22) term by term. In the numerical computation, the sum over s must be stopped at an integer value large enough to provide the required accuracy. Using the orthogonal property of the mode shapes, the reference kinetic energy of the two annular plates is given by

$$T_p = \rho \kappa_\theta \boldsymbol{Q}^{\mathrm{T}} \boldsymbol{Z} \boldsymbol{Q}, \tag{26}$$

where ρ is the mass density of the annular plates, and $\boldsymbol{Z}$ is the $2M \times 2M$ symmetric kinetic energy matrix of the two annular plates written as

$$\boldsymbol{Z} = \begin{bmatrix} \boldsymbol{Z}_1 & \boldsymbol{0} \\ \boldsymbol{0} & \boldsymbol{Z}_2 \end{bmatrix}, \tag{27a}$$

$$Z_{j(i,k)} = \frac{h_j}{2} L_j \delta_{ik}, \quad \delta_{ik}: \text{ Kronecker delta}, \tag{27b}$$

$$L_1 = \int_a^R r W_{ni}^2 \,\mathrm{d}r, \quad L_2 = \int_b^R r W_{ni}^2 \,\mathrm{d}r. \tag{27c,d}$$

The term L_j in Eq. (27b) is obtained by carrying out an integration of Eqs. (27c) and (27d) after inserting Eq. (2) into Eqs. (27c) and (27d):

$$\begin{aligned} L_j = [&S_{1j} + A_{ni}^2 S_{2j} + B_{ni}^2 S_{3j} + C_{ni}^2 S_{4j} + 2(A_{ni} S_{5j} + B_{ni} S_{6j} + C_{ni} S_{7j} + A_{ni} B_{ni} S_{8j} \\ &+ A_{ni} C_{ni} S_{9j} + B_{ni} C_{ni} S_{10j})], \end{aligned} \tag{28}$$

where the coefficients $S_{1j}, S_{2j}, \ldots, S_{10j}$ are listed in Appendix A.

The maximum strain energy of the two annular plates can be computed as a sum of the kinetic energies for each eigenfunction

$$V_p \approx \frac{D_1}{2} \int_0^{2\pi} \int_a^R (\nabla^2 w_1)^2 r \,\mathrm{d}r \,d\theta + \frac{D_2}{2} \int_0^{2\pi} \int_b^R (\nabla^2 w_2)^2 r \,\mathrm{d}r \,\mathrm{d}\theta, \tag{29}$$

where $D_j = Eh_j^3/12(1-\mu^2)$ is the flexural rigidity of the annular plates; μ and E are Poisson's ratio and the modulus of the elasticity of the plates, respectively. Since the value of $(\nabla^2 w_j)^2$ is almost identical to $(\lambda_{ni}^4)_j w_j^2$, the maximum strain energy of the plates becomes

$$V_p = \kappa_\theta \boldsymbol{Q}^{\mathrm{T}} \boldsymbol{H} \boldsymbol{Q}, \tag{30}$$

where $\boldsymbol{H}$ is the $2M \times 2M$ diagonal maximum strain energy matrix of the annular plates given by

$$\boldsymbol{H} = \begin{bmatrix} \boldsymbol{H}_1 & \boldsymbol{0} \\ \boldsymbol{0} & \boldsymbol{H}_2 \end{bmatrix}, \tag{31a}$$

$$H_{j(i,k)} = \frac{(\lambda_{ni}^4)_j}{2} D_j L_j \delta_{ik}. \tag{31b}$$

The natural frequencies and the wet mode shapes of the two annular plates in contact with fluid can be estimated by substituting the reference kinetic energy and the maximum strain energy into Eq. (20) and minimizing the Rayleigh quotient with respect to the unknown coefficients, q_m and p_m:

$$[\boldsymbol{H} - \omega^2(\rho \boldsymbol{Z} + \rho_o \boldsymbol{G})]\boldsymbol{Q} = \{\boldsymbol{0}\}. \tag{32}$$

The determinant of the left-hand side in Eq. (32) must vanish to obtain the nontrivial solution, and then the coupled natural frequency ω of the wet mode can be calculated. Because the matrix $\boldsymbol{G}$ is a function of ω, Eq. (32) cannot be an ordinary eigenvalue problem and the solution of the problem cannot be obtained directly, so an iterative computation is necessary.

3. Example and discussion

3.1. Theoretical and finite element models

To demonstrate the precision of the present method, an example is solved. The fluid-coupled system is composed of two annular plates and water. The annular plates are made of aluminum so that the fluid effect can be strong. The physical properties of the material are as follows: modulus of elasticity = 69.0 GPa, Poisson's ratio = 0.3 and mass density = 2700 kg/m^3. Water as the fluid is in contact with the plates, with a density of 1000 kg/m^3 and a bulk modulus of 2.2 GPa, which is equivalent to a sound speed of 1483 m/s. The viscosity of water is neglected in the theoretical calculation. The upper annular plate has an inner radius of 40 mm, an outer radius of 200 mm, and a thickness of 2.0 mm, while the lower one has an inner radius of 50 mm, an outer radius of 200 mm, and a thickness of 2.5 mm. The distance between the annular plates, d, is 30 mm.

On the basis of the preceding analysis, in order to obtain the natural frequencies of the two annular plates coupled with water, the determinant of the left-hand side in Eq. (32) is calculated by using a commercial software, MathCAD. The characteristic equation derived in the preceding sections involves an infinite and a finite series of algebraic terms. To check the convergence and accuracy of the method, the expansion terms s and m are increased. The expansion term s is set at 300 and the expansion term m for the admissible function is set at 40, which provides a convergent solution in the range of the considered modes. Although Eq. (32) is not an ordinary eigenvalue problem, the calculations can be performed by using an iteration process. The initial frequencies are obtained from the incompressible fluid case which leads to an ordinary eigenvalue problem, and the expected frequency zone was swept to search for the coupled natural frequencies that satisfy Eq. (32) for the compressible fluid case.

Additionally, to check the validity of the theory, a finite element analysis is also carried out for the fluid-coupled system by using a commercial computer code, ANSYS. The finite element model is constructed with the same plate geometry, boundary conditions and material properties used in the theoretical calculation. For the FEM analysis, a two-dimensional axisymmetric model is constructed with harmonic fluid elements (FLUID81) and harmonic shell elements (SHELL61). The fluid element 'FLUID81' with four nodes has three degrees of freedom at each node and it is particularly well suited for calculating hydrostatic pressures and fluid–structure interactions. The shell element 'SHELL61' with two nodes has four degrees of freedom. The fluid domain is divided into a number of identical fluid elements, while the upper and the lower plates are also divided into shell elements. The nodes of the fluid elements at $r = 0$ are constrained in the radial direction only. Additionally, the fluid movement at $r = R$, namely along the rigid

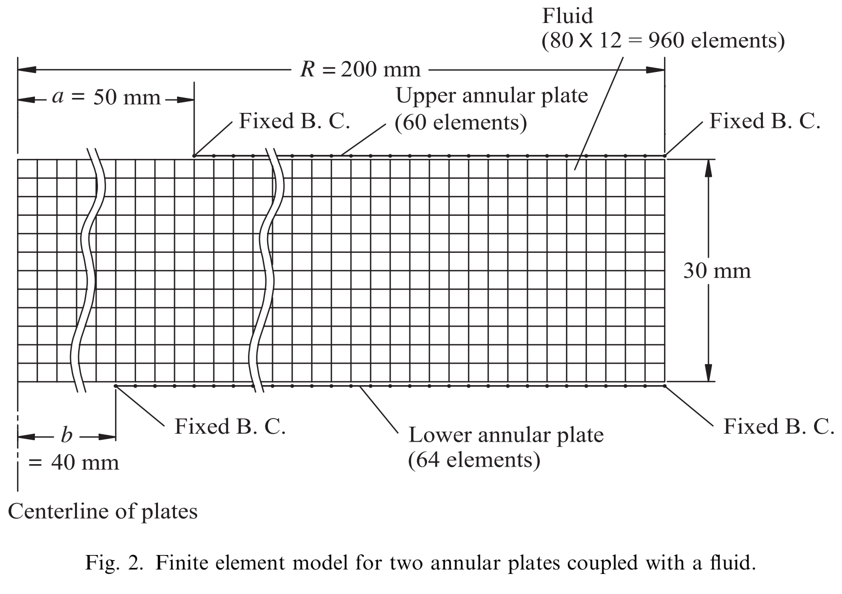

Fig. 2. Finite element model for two annular plates coupled with a fluid.

cylindrical wall, is restricted to the radial direction only, because the vertical velocity of the fluid element nodes adjacent to each surface of the wetted annular plates coincides with that of the plates, so that the finite element model can simulate Eqs. (14a) and (14b). Each annular plate is divided into 60 two-dimensional axisymmetric shell elements of the same size, and the fluid region of the finite element model consists of 960 (12×80) identical fluid elements as illustrated in Fig. 2. All the displacements and rotations are restricted along each plate edge in order to create a clamped boundary condition in the finite element model. In the finite element analysis, the Block Lanczos method is used to extract 50 modal frequencies and the corresponding mode shapes between 20 and 12 000 Hz.

3.2. Theoretical and finite element analysis results

The natural frequencies of the annular plates coupled with water are listed in Table 1 in the range of $0<n<4$ and $1<m'<6$, where m' indicates the number of nodal circles. It is found that the theoretical natural frequencies are in excellent agreement with the finite element results, to within a 0.2% error range when the compressibility of water is taken into account. The mode shapes can be classified into two transverse vibration mode categories according to the relative motion directions between the two annular plates while vibrating; that is, the in-phase and out-of-phase modes, as shown in Fig. 3. However, strictly speaking, these two mode categories cannot become perfect in-phase and out-of-phase modes because the geometries of the two annular plates are not identical. The higher modes can develop into

Table 1
Comparison of the FEM and theoretical natural frequencies for two annular plates coupled with bounded water

Mode		Natural frequency (Hz)			Discrepancy[a] (%)	Mode shape
n	m'	FEM	Theory			
			Incompressible	Compressible		
0	0	—	—	—	—	—
	1	269.9	269.9	270.0	0.04	In-phase
	2	336.5	336.9	336.9	−0.14	Out-of-phase
	3	773.6	774.0	773.6	0.00	In-phase
	4	999.7	1004.0	998.1	0.16	Out-of-phase
	5	1587.4	1589.6	1586.7	0.04	In-phase
1	0	55.3	55.3	55.3	0.00	Out-of-phase
	1	285.1	285.1	285.1	0.00	In-phase
	2	384.2	384.6	383.9	0.08	Out-of-phase
	3	801.2	801.4	801.1	0.01	In-phase
	4	1067.8	1071.0	1066.0	0.17	Out-of-phase
	5	1626.8	1628.4	1625.9	0.06	In-phase
2	0	104.0	104.1	104.0	0.00	Out-of-phase
	1	330.3	330.4	330.4	−0.03	In-phase
	2	465.7	466.2	465.3	0.09	Out-of-phase
	3	873.5	873.8	873.5	0.00	In-phase
	4	1178.2	1181.4	1176.3	0.16	Out-of-phase
	5	1722.9	1724.9	1722.3	0.03	In-phase
3	0	173.3	173.4	173.3	0.00	Out-of-phase
	1	420.6	420.7	420.7	−0.02	In-phase
	2	587.7	588.4	587.4	0.05	Out-of-phase
	3	1003.8	1004.6	1004.0	0.02	In-phase
	4	1335.5	1339.1	1333.6	0.14	Out-of-phase
	5	1888.4	1891.5	1888.1	0.02	In-phase
4	0	271.2	271.4	271.2	0.00	Out-of-phase
	1	555.9	556.3	556.1	−0.04	In-phase
	2	755.0	756.2	754.7	0.04	Out-of-phase
	3	1201.4	1202.9	1201.8	−0.03	In-phase
	4	1544.3	1548.5	1542.5	0.12	Out-of-phase
	5	2136.7	2141.8	2136.9	−0.01	In-phase

Compressible: $c = 1483\,\mathrm{m/s}$; incompressible: $c \to \infty$.

[a] Discrepancy = (FEM−compressible) × 100/FEM.

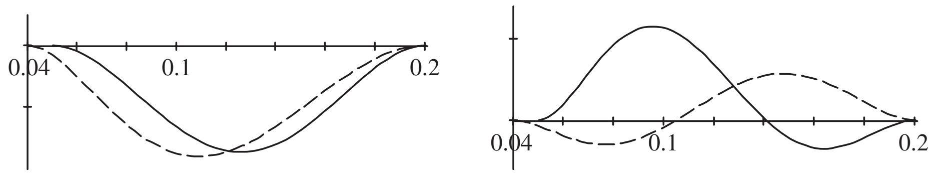

(a) First mode (n = 0, m' = 0)

(b) Second mode (n = 0, m' = 1)

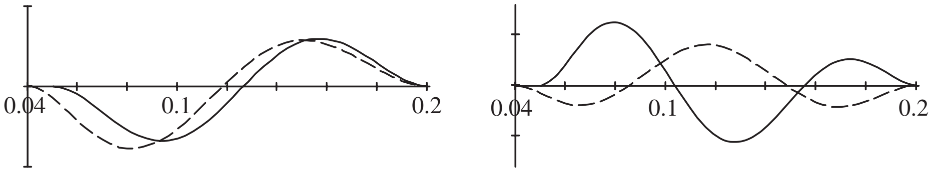

(c) Third mode (n = 0, m' = 1)

(d) Fourth mode (n = 0, m' = 2)

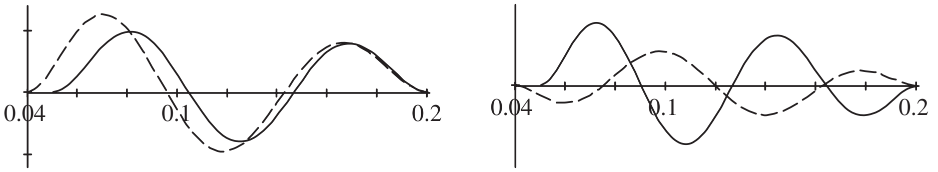

(e) Fifth mode (n = 0, m' = 1)

(f) Sixth mode (n = 0, m' = 2)

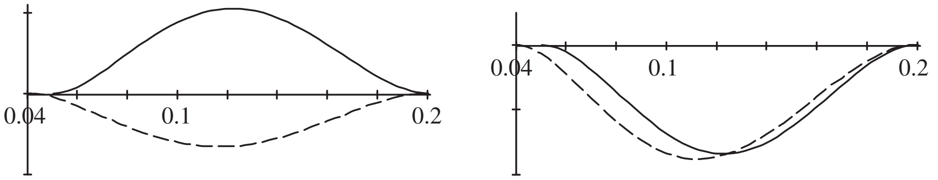

(g) First mode (n = 1, m' = 0)

(h) Second mode (n = 1, m' = 0)

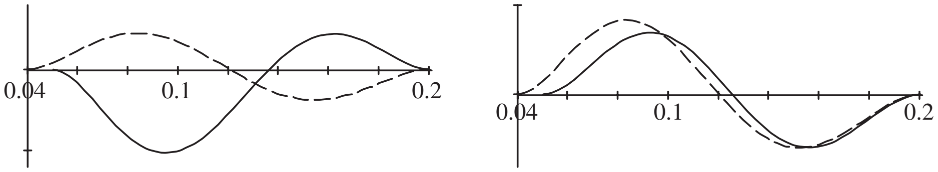

(i) Third mode (n = 1, m' = 1)

(j) Fourth mode (n = 1, m' = 1)

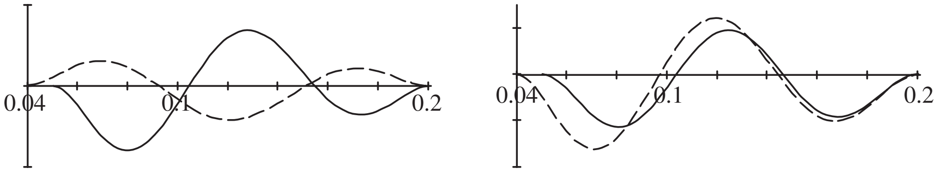

(k) Fifth mode (n = 1, m' = 2)

(l) Sixth mode (n = 1, m' = 2)

Fig. 3. Mode shapes for the two annular plates coupled with a fluid: – – – – –, upper plate; ———, lower plate. (a) First mode ($n = 0$, $m' = 0$), (b) second mode ($n = 0$, $m' = 1$), (c) third mode ($n = 0$, $m' = 1$), (d) fourth mode ($n = 0$, $m' = 2$), (e) fifth mode ($n = 0$, $m' = 1$), (f) sixth mode ($n = 0$, $m' = 2$).

mixed modes which cannot be categorized as in-phase or out-of-phase modes. As shown in Fig. 3, the difference in the plate maximum deflection between the two plates is not dominant in the in-phase modes, because the movement of one plate contributes to that of the other plate owing to transverse movement of the fluid. On the contrary, the difference in the plate deflection for the out-of-phase modes is greater than that of the in-phase modes, because the deflection of one of the annular plates tends to hinder the deflection of the other plate through the fluid. Therefore, the maximum deflection of the more flexible plate is greater than that of the stiffer one. Fig. 4 shows typical displacement vector plots when identical annular plates with $d = 50$ mm are coupled with water for $n = 0$. The first mode corresponds to the in-phase mode where the major fluid displacement vectors tend to move in the transverse direction, while the second mode

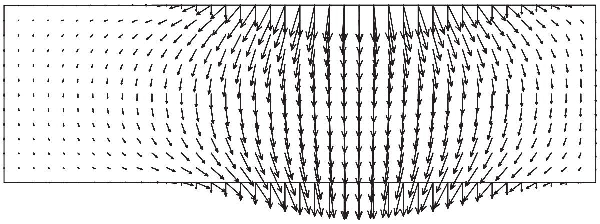

1st mode ($m' = 0$, in–phase mode)

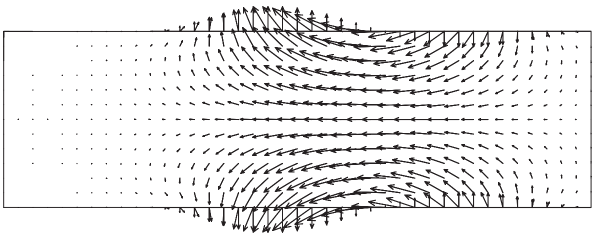

2nd mode ($m' = 0$, out–of–phase mode)

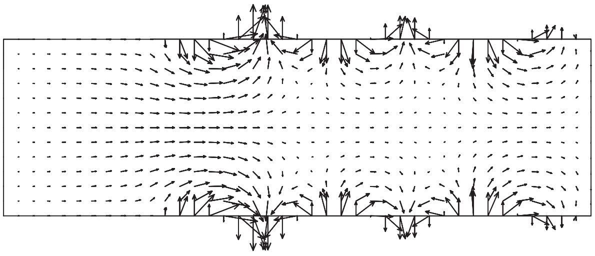

11th mode ($m' = 5$, out–of–phase mode)

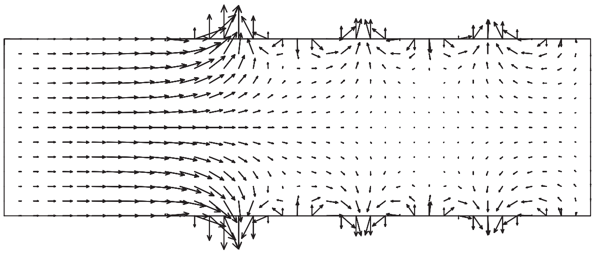

12th mode ($m' = 5$, out–of–phase mode)

Fig. 4. Displacement vector plots of typical mode shapes with $n = 0$, $a = b = d = 50$ mm and $c = 1483$ m/s. First mode ($m' = 0$, in-phase mode), 2nd mode ($m' = 0$, out-of-phase mode), 11th mode ($m' = 5$, out-of-phase mode), 12th mode ($m' = 5$, out-of-phase mode).

corresponds to the out-of-phase mode where the major vectors of the fluid displacement tend to move in the lateral direction. The difference in the fluid movement vectors creates a change in the natural frequency. Furthermore, the fluid movement is localized into several regions according to an increase in the number of nodal circles or nodal diameters, and the characteristics of the fluid flow direction become indistinct. The natural frequency difference between the in-phase and out-of-phase modes is gradually reduced as the number of nodal circles or nodal diameters is increased. The normalized natural frequency, defined as the natural frequency of the structure in contact with fluid divided by the corresponding natural frequency in air, increases with an increase of the number of nodal circles or nodal diameters.

The 11th and 12th modes show out-of-phase modes with five nodal circles as illustrated in Fig. 4. The fluid displacement is predominant near the surfaces of the two plates in both modes. Although the 11th and 12th modes have the same number of nodal circles, the fluid displacement patterns are different and the nodal circle points do not coincide. In the 12th mode, a fluid surge appears near the inner edge, induced by fluid compressibility. It is observed that the fluid surge (or concentration) at a fluid region far from the structure due to compressibility appears more frequently in the higher out-of-phase modes. The various abnormal mode shapes with fluid surge are similar to the 12th mode of Fig. 4, in accordance with the increase in fluid compressibility.

3.3. *Effects of the distance between the annular plates*

Figs. 5–8 illustrate the effects of the distance between the two annular plates on the fluid-coupled natural frequencies, when the geometry and the material property of the two plates are identical to each other. It is well known that the natural frequency of the plate in contact with fluid is always less than that of the corresponding dry mode, due to the contribution of a hydrodynamic mass [e.g., Païdoussis, 2004]. Hence, the normalized natural frequency always lies between unity and zero. As shown in Figs. 5 and 7, the normalized natural frequency of the out-of-phase modes gradually increases with an increase of the number of nodal diameters (n) or nodal circles (m') by virtue of a localization (or division) of the fluid flow. The normalized natural frequencies increase and eventually converge to specific values, which are equivalent to the case of infinite distance between the plates. For a fixed distance ratio (d/R), the normalized natural frequency decreases as the number of nodal circles decreases. Convergence occurs at a smaller distance ratio (d/R) as the number of nodal circles increases. On the contrary, the normalized natural frequencies decrease and also converge to specific values, which are equivalent to the case of infinite distance between the plates with an increase in d/R for the in-phase modes as illustrated in Figs. 6 and 8. A small fluid thickness reduces the natural frequencies drastically for the out-of-phase modes, while the normalized natural frequencies increase sharply with a decrease of d/R for the in-phase modes. Similarly, the normalized natural frequencies increase with an increase of the number of nodal circles (n) for the fixed m' due to the fluid flow localization or division regardless of the modal category (in-phase modes and out-of-phase modes). As d/R increases, the normalized natural frequencies of the corresponding in-phase and out-of-phase modes will approach and merge with each other in the infinite fluid case.

3.4. *Effects of the inner radius*

The inner radius effects on the normalized natural frequencies for $n = 0$ and 1 are shown in Figs. 9 and 10, respectively, where the two plates coupled with water have the same geometry and the same material properties, so $a = b$ and $d = 30\,\text{mm}$. The inner radius effect on the normalized natural frequencies is not negligible except for $m' = 0$ as illustrated in Figs. 9 and 10. This fact can be explained as follows: generally, the normalized frequency of a bluff body can be expressed as

$$\frac{\omega}{\omega_a} = \sqrt{\frac{1}{1 + M_f/M}}, \tag{33}$$

where ω_a is the natural frequency of the dry mode; M_f and M are the hydrodynamic mass (or added mass) and the structural mass, respectively. When the inner radius of the two plates increases and the outer diameter is fixed, the mass of the plates will be reduced by a square of the plate radius, and concurrently, the fluid-contacting area will also decrease at the same rate. Therefore, M_f/M is approximately constant, regardless of the inner radius. The normalized natural frequency (ω/ω_a) will not change according to the inner radius, since the vibration mode with $m' = 0$ is very close to the vibration mode of a bluff body. When the number of the nodal circles (m') increases, M_f/M decreases by the localization of the fluid flow, and finally the normalized natural frequencies increase by increasing the inner radius, regardless of modal category, when the outer radius of the two plates is fixed.

3.5. *Effects of the compressibility*

A further comparison is made for an investigation of fluid compressibility effects on the coupled natural frequencies. Figs. 11 and 12 show the natural frequencies of the in-phase and the out-of-phase modes obtained, respectively, by the ANSYS analysis for $n = 0$. Since several modes with the same number of nodal circles can appear as in Fig. 4, when the fluid compressibility increases, the radial modes are arranged in order of the serial mode instead of m' in Figs. 11 and 12. When the sound speed changes from $c = 1483$ to $148.3\,\text{m/s}$, the natural frequencies of the in-phase mode decreases as shown Fig. 11. Especially, the natural frequency drop of the higher radial modes is greater than that of the lower radial modes. The frequency drop of the in-phase modes for $c > 500\,\text{m/s}$ is negligible between the first mode and the fourth mode. The frequency drop of the out-of-phase modes is remarkable for the higher radial modes when compared

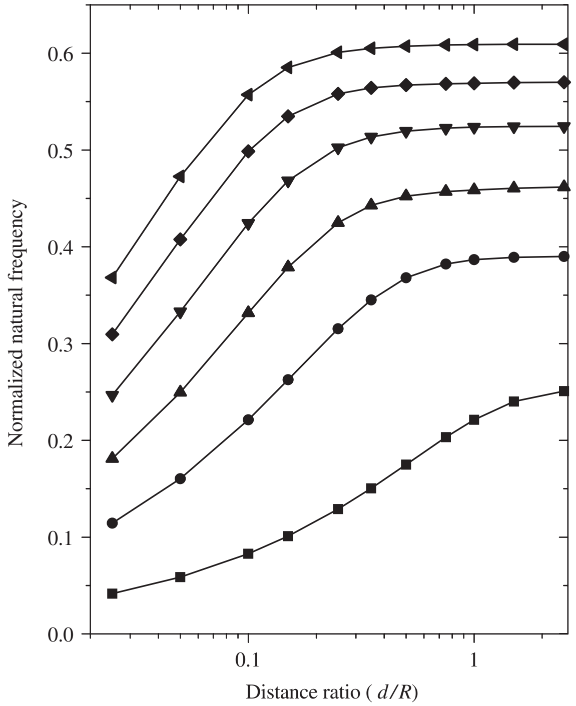

Fig. 5. Normalized natural frequency of the two identical annular plates coupled with water for the out-of-phase mode with $n = 1$: –■–, $m' = 0$; –●–, $m' = 1$; –▲–, $m' = 2$; –▼–, $m' = 3$; –◆–, $m' = 4$; –◀–, $m' = 5$.

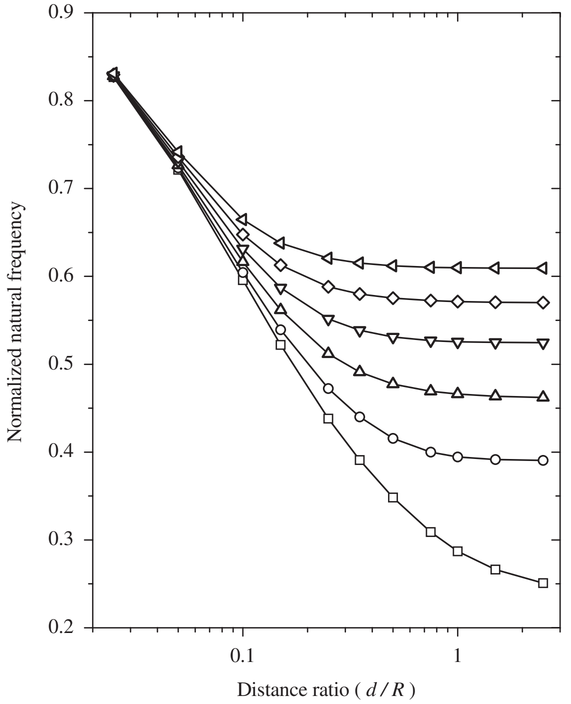

Fig. 6. Normalized natural frequency of the two identical annular plates coupled with water for the in-phase mode with $n = 1$: –□–, $m' = 0$; –○–, $m' = 1$; –△–, $m' = 2$; –▽–, $m' = 3$; –◇–, $m' = 4$; –◁–, $m' = 5$.

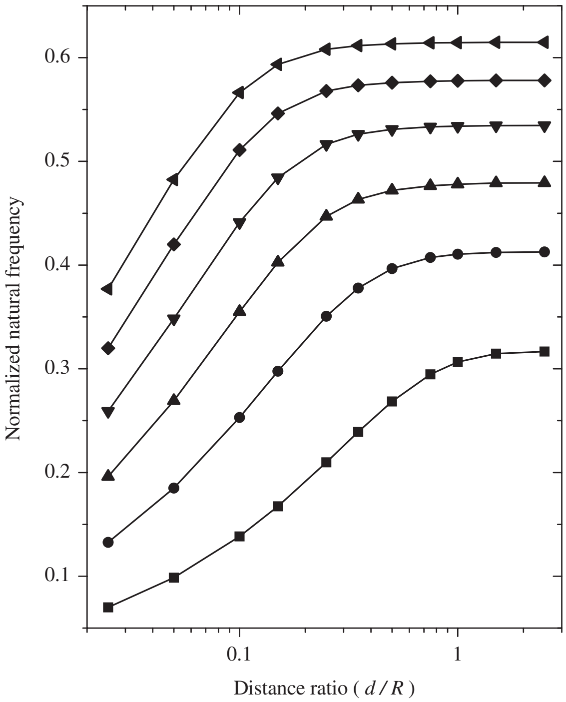

Fig. 7. Normalized natural frequency of the two identical annular plates coupled with water for the out-of-phase mode with $n = 2$. Key as in Fig. 5.

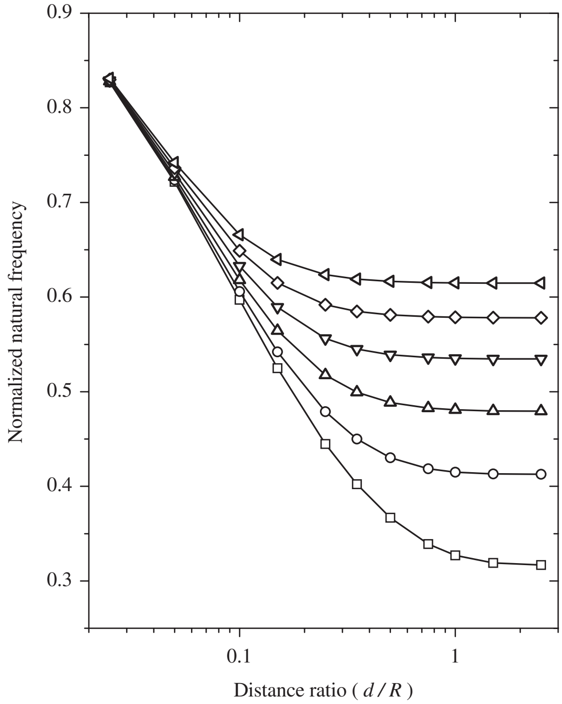

Fig. 8. Normalized natural frequency of the two identical annular plates coupled with water for the in-phase mode with $n = 2$. Key as in Fig. 6.

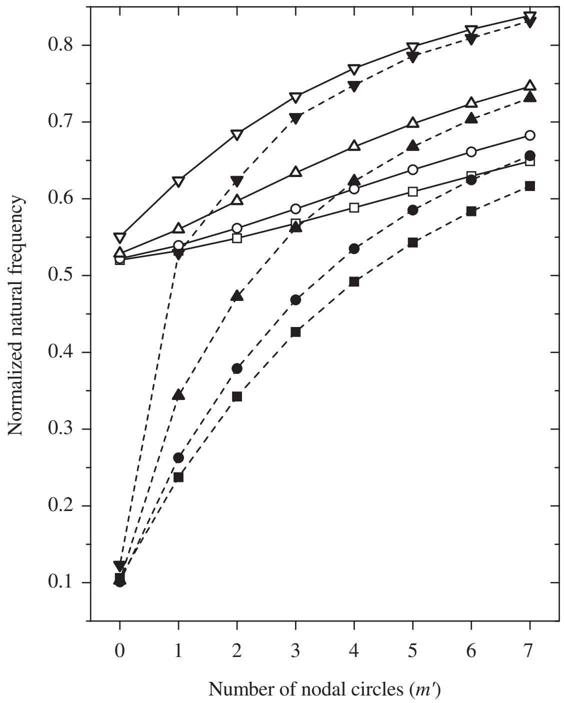

Fig. 9. Inner radius effect on the normalized natural frequency of the two identical annular plates coupled with water for $n = 1$ and $d = 30$ mm: –□–, in-phase mode, $a = 10$ mm; –○–, $a = 50$ mm; –△–, $a = 100$ mm; –▽–, $a = 150$ mm: – –■– –, out-of-phase mode, $a = 10$ mm; – –●– –, $a = 50$ mm; – –▲– –, $a = 100$ mm; – –▼– –, $a = 150$ mm.

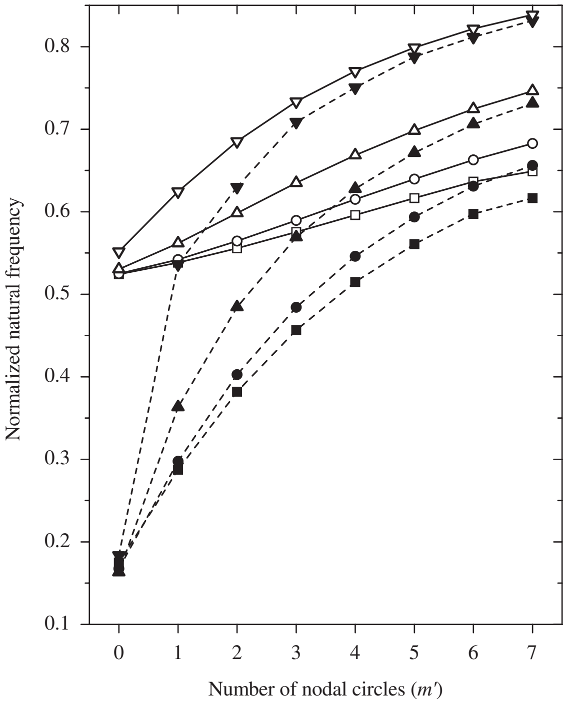

Fig. 10. Inner radius effect on the normalized natural frequency of the two identical annular plates coupled with water for $n = 2$ and $d = 30$ mm. Key as in Fig. 9.

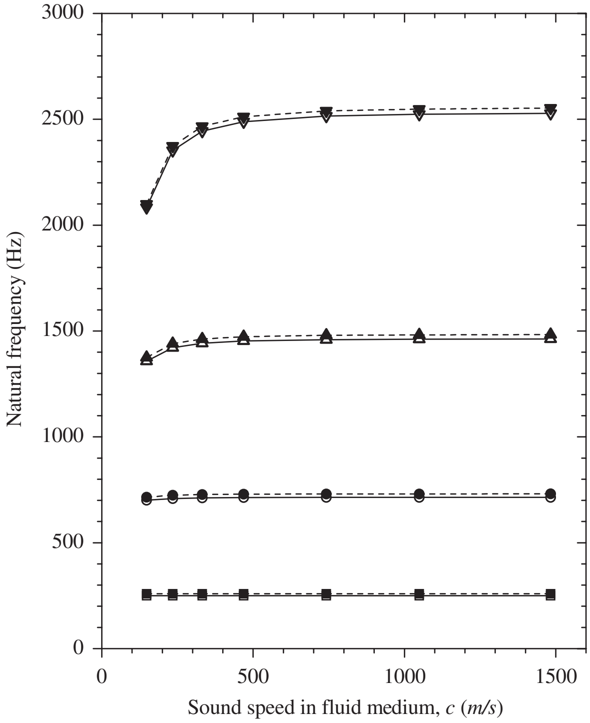

Fig. 11. Compressibility effect on the natural frequency of the two identical annular plates coupled with a compressible fluid for the in-phase modes (–□–, first mode; –○–, second mode; –△–, third mode; –▽–, fourth mode for $n = 0$: – –■– –, first mode; – –●– –, second mode; – –▲– –, third mode; – –▼– –, fourth mode for $n = 1$).

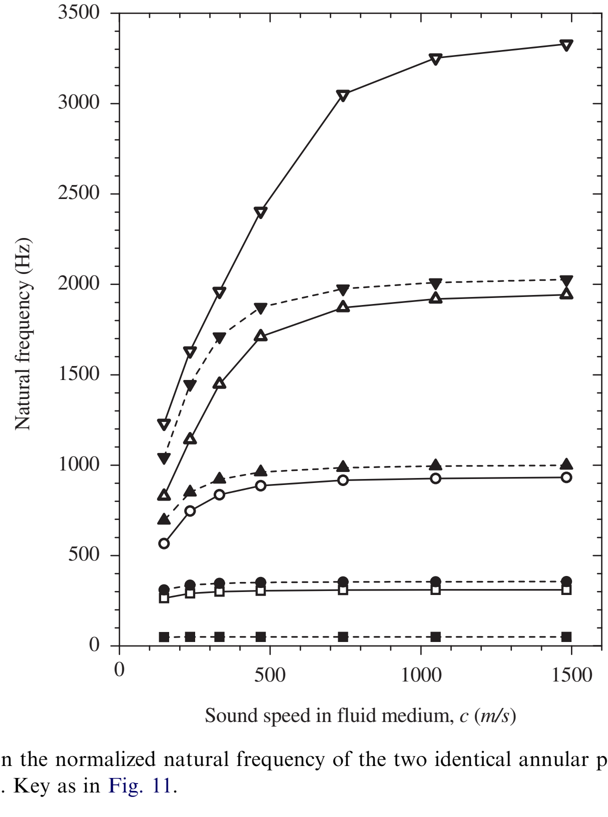

Fig. 12. Compressibility effect on the normalized natural frequency of the two identical annular plates coupled with a compressible fluid for the out-of-phase modes. Key as in Fig. 11.

with that of the in-phase modes, as illustrated in Fig. 12. That is to say, the fluid compressibility affects the out-of-phase modes rather than the in-phase modes and it also affects the higher radial modes. Several abnormal mode shapes which deviated from the dry mode shape are observed in the higher out-of-phase modes for the compressible fluid.

4. Conclusions

An analytical method to estimate the natural frequencies of two unequal annular plates coupled with a compressible fluid is developed using the Rayleigh–Ritz method and the finite Hankel transform. It is observed that the two sets of modes, the so-called out-of-phase and in-phase modes, are obtained alternately in the fluid-coupled system and these modes gradually can shift to mixed modes according to the geometric differences between the two annular plates. It is verified that this theoretical approach can predict the coupled natural frequencies excellently. It is also found that the normalized natural frequency of the out-of-phase modes increases and converges to a specific value as the distance ratio (d/R) decreases, regardless of the number of nodal circles (m'), while those of the in-phase modes decrease, owing to the localization (or division) of the fluid flow. It is also observed that the inner radius does not affect the normalized natural frequencies for $m' = 0$ in the case of a fixed nodal diameter, and the fluid compressibility affects the out-of-phase modes and the higher modes rather than the in-phase modes and the lower modes.

Appendix A

A.1. Coefficients for the mode shapes

$$\begin{aligned}
A_{nm} = \frac{1}{T_{nm}}[&\{\mathrm{I}'_n(\lambda_{nm}a)\mathrm{K}_n(\lambda_{nm}R) - \mathrm{I}_n(\lambda_{nm}R)\mathrm{K}'_n(\lambda_{nm}a)\}\mathrm{J}_n(\lambda_{nm}a) \\
&+ \{\mathrm{I}_n(\lambda_{nm}a)\mathrm{K}'_n(\lambda_{nm}a) - \mathrm{I}'_n(\lambda_{nm}a)\mathrm{K}_n(\lambda_{nm}a)\}\mathrm{J}_n(\lambda_{nm}R) \\
&+ \{\mathrm{I}_n(\lambda_{nm}R)K_n(\lambda_{nm}a) - \mathrm{I}_n(\lambda_{nm}a)\mathrm{K}_n(\lambda_{nm}R)\}\mathrm{J}'_n(\lambda_{nm}a)],
\end{aligned}$$

$$\begin{aligned}
B_{nm} = \frac{1}{T_{nm}}[&\{\mathrm{Y}_n(\lambda_{nm}R)\mathrm{K}'_n(\lambda_{nm}a) - \mathrm{Y}'_n(\lambda_{nm}a)\mathrm{K}_n(\lambda_{nm}R)\}\mathrm{J}_n(\lambda_{nm}\, a) \\
&+ \{\mathrm{Y}'_n(\lambda_{nm}a)\mathrm{K}_n(\lambda_{nm}a) - \mathrm{Y}_n(\lambda_{nm}a)\mathrm{K}'_n(\lambda_{nm}a)\}\mathrm{J}_n(\lambda_{nm}R) \\
&+ \{\mathrm{Y}_n(\lambda_{nm}a)\mathrm{K}_n(\lambda_{nm}R) - \mathrm{Y}_n(\lambda_{nm}R)\mathrm{K}_n(\lambda_{nm}a)\}\mathrm{J}'_n(\lambda_{nm}a)],
\end{aligned}$$

$$\begin{aligned}
C_{nm} = \frac{1}{T_{nm}}[&\{\mathrm{I}_n(\lambda_{nm}R)\mathrm{Y}'_n(\lambda_{nm}R) - \mathrm{I}'_n(\lambda_{nm}a)\mathrm{Y}_n(\lambda_{nm}R)\}\mathrm{J}_n(\lambda_{nm}a) \\
&+ \{\mathrm{I}'_n(\lambda_{nm}a)\mathrm{Y}_n(\lambda_{nm}a) - \mathrm{I}_n(\lambda_{nm}a)\mathrm{Y}'_n(\lambda_{nm}a)\}\mathrm{J}_n(\lambda_{nm}R) \\
&+ \{\mathrm{I}_n(\lambda_{nm}a)\mathrm{Y}_n(\lambda_{nm}R) - \mathrm{I}_n(\lambda_{nm}R)\mathrm{Y}_n(\lambda_{nm}a)\}\mathrm{J}'_n(\lambda_{nm}a)],
\end{aligned}$$

$$\begin{aligned}
T_{nm} = {}&\mathrm{I}_n(\lambda_{nm}R)\mathrm{K}'_n(\lambda_{nm}a)\mathrm{Y}_n(\lambda_{nm}a) - \mathrm{I}'_n(\lambda_{nm}a)\mathrm{K}_n(\lambda_{nm}R)\mathrm{Y}_n(\lambda_{nm}a) \\
&- \mathrm{I}_n(\lambda_{nm}R)\mathrm{K}_n(\lambda_{nm}a)\mathrm{Y}'_n(\lambda_{nm}a) + \mathrm{I}_n(\lambda_{nm}a)\mathrm{K}_n(\lambda_{nm}R)\mathrm{Y}'_n(\lambda_{nm}a) \\
&+ \mathrm{I}'_n(\lambda_{nm}a)\mathrm{K}_n(\lambda_{nm}a)\mathrm{Y}_n(\lambda_{nm}R) - \mathrm{I}_n(\lambda_{nm}a)\mathrm{K}'_n(\lambda_{nm}a)\mathrm{Y}_n(\lambda_{nm}R),
\end{aligned}$$

A.2. Coefficients for the integration

$$\xi 1_{nms} = \left(\frac{1}{\beta_{ns}^2 - \lambda_{nm}^2}\right), \quad \xi 2_{nms} = \left(\frac{1}{\beta_{ns}^2 + \lambda_{nm}^2}\right),$$

$$\begin{aligned}
\Lambda 1_{nms} &= \int_a^R \mathrm{J}_n(\lambda_{nm}r)\mathrm{J}_n(\beta_{ns}r)r\,\mathrm{d}r \\
&= \xi 1_{nms}\left\{\begin{array}{l} (\lambda_{nm}R)\mathrm{J}_n(\beta_{ns}R)\mathrm{J}'_n(\lambda_{nm}R) - (\lambda_{nm}a)\mathrm{J}_n(\beta_{ns}\, a)\mathrm{J}'_n(\lambda_{nm}a) \\ \quad +(\beta_{ns}a)\mathrm{J}_n(\lambda_{nm}a)\mathrm{J}'_n(\beta_{ns}a) \end{array}\right\},
\end{aligned}$$

$$\Lambda 2_{nms} = \int_a^R \mathrm{Y}_n(\lambda_{nm} r)\mathrm{J}_n(\beta_{ns} r) r\,\mathrm{d}r$$
$$= \xi 1_{nms} \left\{ \begin{array}{l} (\lambda_{nm}R)\mathrm{J}_n(\beta_{ns}R)\mathrm{Y}_n'(\lambda_{nm}R) - (\lambda_{nm}a)\mathrm{J}_n(\beta_{ns}a)\mathrm{Y}_n'(\lambda_{nm}a) \\ \quad +(\beta_{ns}a)\mathrm{Y}_n(\lambda_{nm}a)\mathrm{J}_n'(\beta_{ns}a), \end{array} \right\},$$

$$\Lambda 3_{nms} = \int_a^R \mathrm{I}_n(\lambda_{nm} r)\mathrm{J}_n(\beta_{ns} r) r\,\mathrm{d}r$$
$$= \xi 2_{nms} \left\{ \begin{array}{l} (\lambda_{nm}R)\mathrm{J}_n(\beta_{ns}R)\mathrm{I}_n'(\lambda_{nm}R) - (\lambda_{nm}a)\mathrm{J}_n(\beta_{ns}a)\mathrm{I}_n'(\lambda_{nm}a) \\ +(\beta_{ns}a)\mathrm{I}_n(\lambda_{nm}a)\mathrm{J}_n'(\beta_{ns}a) \end{array} \right\},$$

$$\Lambda 4_{nms} = \int_a^R \mathrm{K}_n(\lambda_{nm} r)\mathrm{J}_n(\beta_{ns} r) r\,\mathrm{d}r$$
$$= \xi 2_{nms} \left\{ \begin{array}{l} (\lambda_{nm}R)\mathrm{J}_n(\beta_{ns}R)\mathrm{K}_n'(\lambda_{nm}R) - (\lambda_{nm}a)\mathrm{J}_n(\beta_{ns}a)\mathrm{K}_n'(\lambda_{nm}a) \\ +(\beta_{ns}a)\mathrm{K}_n(\lambda_{nm}a)\mathrm{J}_n'(\beta_{ns}a) \end{array} \right\},$$

$$H_{ns} = \int_0^R \{\mathrm{J}_n(\beta_{ns} r)\}^2 r\,\mathrm{d}r = \frac{R^2}{2}\left\{1 - \frac{n^2}{(\beta_{ns}R)^2}\right\}\{\mathrm{J}_n(\beta_{ns}R)\}^2,$$

$$S_{1m} = \frac{R^2}{2}\left[\{\mathrm{J}_n'(\lambda_{nm}R)\}^2 + \left\{1 - \frac{n^2}{(\lambda_{nm}R)^2}\right\}\{\mathrm{J}_n(\lambda_{nm}R)\}^2\right]$$
$$- \frac{a^2}{2}\left[\{\mathrm{J}_n'(\lambda_{nm}a)\}^2 + \left\{1 - \frac{n^2}{(\lambda_{nm}a)^2}\right\}\{\mathrm{J}_n(\lambda_{nm}a)\}^2\right],$$

$$S_{2m} = \frac{R^2}{2}\left[\{\mathrm{Y}_n'(\lambda_{nm}R)\}^2 + \left\{1 - \frac{n^2}{(\lambda_{nm}R)^2}\right\}\{\mathrm{Y}_n(\lambda_{nm}R)\}^2\right]$$
$$- \frac{a^2}{2}\left[\{\mathrm{Y}_n'(\lambda_{nm}a)\}^2 + \left\{1 - \frac{n^2}{(\lambda_{nm}a)^2}\right\}\{\mathrm{Y}_n(\lambda_{nm}a)\}^2\right],$$

$$S_{3m} = -\frac{R^2}{2}\left[\{\mathrm{I}_n'(\lambda_{nm}R)\}^2 - \left\{1 + \frac{n^2}{(\lambda_{nm}R)^2}\right\}\{\mathrm{I}_n(\lambda_{nm}R)\}^2\right]$$
$$+ \frac{a^2}{2}\left[\{\mathrm{I}_n'(\lambda_{nm}a)\}^2 - \left\{1 + \frac{n^2}{(\lambda_{nm}a)^2}\right\}\{\mathrm{I}_n(\lambda_{nm}a)\}^2\right],$$

$$S_{4m} = -\frac{R^2}{2}\left[\{\mathrm{K}_n'(\lambda_{nm}R)\}^2 - \left\{1 + \frac{n^2}{(\lambda_{nm}R)^2}\right\}\{\mathrm{K}_n(\lambda_{nm}R)\}^2\right]$$
$$+ \frac{a^2}{2}\left[\{\mathrm{K}_n'(\lambda_{nm}a)\}^2 - \left\{1 + \frac{n^2}{(\lambda_{nm}a)^2}\right\}\{\mathrm{K}_n(\lambda_{nm}a)\}^2\right],$$

$$S_{5m} = \frac{R^2}{2}\left[\mathrm{J}_n'(\lambda_{nm}R)\mathrm{Y}_n'(\lambda_{nm}R) + \left\{1 - \frac{n^2}{(\lambda_{nm}R)^2}\right\}\mathrm{J}_n(\lambda_{nm}R)\mathrm{Y}_n(\lambda_{nm}R)\right]$$
$$- \frac{a^2}{2}\left[\mathrm{J}_n'(\lambda_{nm}a)\mathrm{Y}_n'(\lambda_{nm}a) + \left\{1 - \frac{n^2}{(\lambda_{nm}a)^2}\right\}\mathrm{J}_n(\lambda_{nm}a)\mathrm{Y}_n(\lambda_{nm}a)\right],$$

$$S_{6m} = \frac{R^2}{2(\lambda_{nm}R)}[\mathrm{J}_n(\lambda_{nm}R)\mathrm{I}_n'(\lambda_{nm}R) - \mathrm{I}_n(\lambda_{nm}R)\mathrm{J}_n'(\lambda_{nm}R)]$$
$$- \frac{a^2}{2(\lambda_{nm}a)}[\mathrm{J}_n(\lambda_{nm}a)\mathrm{I}_n'(\lambda_{nm}a) - \mathrm{I}_n(\lambda_{nm}a)\mathrm{J}_n'(\lambda_{nm}a)],$$

$$S_{7m} = \frac{R^2}{2(\lambda_{nm}R)}[\mathrm{J}_n(\lambda_{nm}R)\mathrm{K}'_n(\lambda_{nm}R) - \mathrm{K}_n(\lambda_{nm}R)\mathrm{J}'_n(\lambda_{nm}R)] - \frac{a^2}{2(\lambda_{nm}a)}[\mathrm{J}_n(\lambda_{nm}a)\mathrm{K}'_n(\lambda_{nm}a) - \mathrm{K}_n(\lambda_{nm}a)\mathrm{J}'_n(\lambda_{nm}a)],$$

$$S_{8m} = \frac{R^2}{2(\lambda_{nm}R)}[\mathrm{Y}_n(\lambda_{nm}R)\mathrm{I}'_n(\lambda_{nm}R) - \mathrm{I}_n(\lambda_{nm}R)\mathrm{Y}'_n(\lambda_{nm}R)] - \frac{a^2}{2(\lambda_{nm}a)}[\mathrm{Y}_n(\lambda_{nm}a)\mathrm{I}'_n(\lambda_{nm}a) - \mathrm{I}_n(\lambda_{nm}a)\mathrm{Y}'_n(\lambda_{nm}a)],$$

$$S_{9m} = \frac{R^2}{2(\lambda_{nm}R)}[\mathrm{Y}_n(\lambda_{nm}R)\mathrm{K}'_n(\lambda_{nm}R) - \mathrm{K}_n(\lambda_{nm}R)\mathrm{Y}'_n(\lambda_{nm}R)] - \frac{a^2}{2(\lambda_{nm}a)}[\mathrm{Y}_n(\lambda_{nm}a)\mathrm{K}'_n(\lambda_{nm}a) - \mathrm{K}_n(\lambda_{nm}a)\mathrm{Y}'_n(\lambda_{nm}a)],$$

$$S_{10m} = -\frac{R^2}{2}\left[\mathrm{K}'_n(\lambda_{nm}R)\mathrm{I}'_n(\lambda_{nm}R) - \left\{1 + \frac{n^2}{(\lambda_{nm}R)^2}\right\}\mathrm{K}_n(\lambda_{nm}R)\mathrm{I}_n(\lambda_{nm}R)\right] + \frac{a^2}{2}\left[\mathrm{K}'_n(\lambda_{nm}a)\mathrm{I}'_n(\lambda_{nm}a) - \left\{1 + \frac{n^2}{(\lambda_{nm}a)^2}\right\}\mathrm{K}_n(\lambda_{nm}a)\mathrm{I}_n(\lambda_{nm}a)\right].$$

References

Amabili, M., 1996. Effect of finite fluid depth on the hydroelastic vibrations of circular and annular plates. Journal of Sound and Vibration 193 (4), 909–925.

Amabili, M., 2000a. Vibration of fluid-filled hermetic cans. Journal of Fluids and Structures 14 (2), 235–255.

Amabili, M., 2000b. Eigenvalue problems for vibrating structures coupled with quiescent fluids with free surface. Journal of Sound and Vibration 231 (1), 79–97.

Amabili, M., Dalpiaz, G., 1998. Vibrations of base plates in annular cylindrical tanks: theory and experiments. Journal of Sound and Vibration 210 (3), 329–350.

Amabili, M., Frosali, G., Kwak, M.K., 1996. Free vibrations of annular plates coupled with fluids. Journal of Sound and Vibration 191 (5), 825–846.

Biswal, K.C., Bhattacharyya, S.K., Sinha, P.K., 2004. Dynamic response analysis of a liquid-filled cylindrical tank with annular baffle. Journal of Sound and Vibration 274 (1–2), 13–37.

Cho, J.R., Lee, H.W., Kim, K.W., 2002. Free vibration analysis of baffled liquid-storage tanks by the structural–acoustic finite element formulation. Journal of Sound and Vibration 258 (5), 847–866.

Jeong, K.H., 2003. Free vibration of two identical circular plates coupled with bounded fluid. Journal of Sound and Vibration 260 (4), 653–670.

Jeong, K.H., Kim, K.J., 2005. Hydroelastic vibration of a circular plate submerged in a bounded compressible fluid. Journal of Sound and Vibration 283 (1–2), 153–172.

Jeong, K.H., Lee, G.M., Park, K.B., Jhung, M.J., 2001. Hydroelastic vibration of multiple circular plates coupled with fluid. In: Proceedings of the First International Structural Engineering and Construction Conference, Honolulu, Hawaii, pp. 705–710.

Kasahara, M., Ishii, H., Takagi, M., Kawamoto, K., 1994. An analysis of fluid structure coupled vibration considering modal added mass. Journal of the Japan Society of Mechanical Engineers (C) 60 (571), 743–748 (in Japanese).

Kim, Y.W., Lee, Y.S., 2005. Coupled vibration analysis of liquid-filled rigid cylindrical storage tank with an annular plate cover. Journal of Sound and Vibration 279 (1–2), 217–235.

Kwak, M.K., Amabili, M., 1999. Hydroelastic vibration of free-edge annular plates. ASME Journal of Vibration and Acoustics 121, 26–32.

Liang, C.C., Tai, Y.S., Li, P.L., 1999. Natural frequencies of annular plates having contact with fluid. Journal of Sound and Vibration 228 (5), 1167–1181.

Païdoussis, M.P., 2004. Fluid–Structure Interaction: Slender Structures and Axial Flow, vol. 2. Elsevier Academic Press, London.

Zhu, F., 1994. Rayleigh quotients for coupled free vibration. Journal of Sound and Vibration 171 (5), 641–649.